Study of EEGs from Somatosensory Cortex and Alzheimer 's Disease Sources

Md R. Bashar, Yan Li, and Peng Wen

Abstract—This study is to investigate the electroencephalogram (EEG) differences generated from a normal and Alzheimer's disease (AD) sources. We also investigate the effects of brain tissue distortions due to AD on EEG. We develop a realistic head model from T1 weighted magnetic resonance imaging (MRI) using finite element method (FEM) for normal source (somatosensory cortex (SC) in parietal lobe) and AD sources (right amygdala (RA) and left amygdala (LA) in medial temporal lobe). Then, we compare the AD sourced EEGs to the SC sourced EEG for studying the nature of potential changes due to sources and 5% to 20% brain tissue distortions. We find an average of 0.15 magnification errors produced by AD sourced EEGs. Different brain tissue distortion models also generate the maximum 0.07 magnification. EEGs obtained from AD sources and different brain tissue distortion levels vary scalp potentials from normal source, and the electrodes residing in parietal and temporal lobes are more sensitive than other electrodes for AD sourced EEG.

Keywords—Alzheimer's disease (AD), Brain tissue distortion, Electroencephalogram, Finite element method.

I. INTRODUCTION

A LZHEIMER'S disease (AD) [1-8] is one of the challenging research areas to brain scientist or decades. AD is a neurodegenerative disorder which alters the structural and functional brain activities. Therefore, it is important to detect AD as early as possible because treatment may be the most effective, if introduced earlier. In practice, the diagnosis of AD is largely based on clinical history and different examinations supported by neuropsychological evidence of the pattern of cognitive impairments [1]. However, in reality, only fifty percentage of probable AD is detected in the primary case.

The reason and progression of AD are not well understood so far. Primarily, some investigation indicates that the disease is associated with plaques and tangles in the brain. Plaques are extra cellular deposits of amyloid the gray matter (GM) of the brain. The plaques are flexible in shape and size, but are on the average of 50 μm. The number of people with plaques almost linearly increases after the age of 60. Tangles are formed by a kind of protein, known as tau causing it to aggregate in an insoluble form. Based on aggregating of proteins into GM tissues of brain, dementia (caused by AD) is characterized into four classes: predementia, early dementia, moderate dementia and advanced dementia. Predementia, the first symptoms of AD are often mistaken as related to aging or stress. Early dementia leads to difficulties with language, executive functions or movements and perception. These symptoms are more prominent than memory problems. Speech difficulties become evident due to an inability to recall vocabulary, which leads to frequent incorrect word substitutions in moderate dementia. Advanced dementia is the last step of neurological disorders

To develop prevention treatment for AD, it is necessary to identify early biological markers for AD prediction. The best recognized *in vivo* markers of AD are measures of brain structure and function as obtained with neuroimaging [2]. Structural imaging with either computer tomography (CT) or T1 weighted magnetic resonance imaging (MRI) allows brain atrophy to be assessed in *in vivo* [3]. Different studies [3,4] in the early stages of AD have consistently reported that, the first brain region to be affected by atrophy is the medial temporal lobe, which comprises with hippocampus proper, the para hippocampal gyrus and the amygdala. The study by Chupin *et al.* [5] are also consistent regarding the sources of AD. They performed the segmentation of hippocampus and amygdala for constrained region deformation by AD. EEG has an important role in the evaluation of certain neurological disorders based on their criteria. Most studies [6,7] analyze event related potentials (ERPs) of EEG recorded from different candidates and controls to diagnosis early detection of AD. Topographic maps of the spectral power of EEG provide information that helps differentiating neurological disorders for various neurological cases. Other studies [1,8] perform MRI segmentation scanned from candidates and controls to show the changes of GM inside the brain to diagnosis of AD and to understand its severity.

In this study, we aim to show: (1) the feasibility to improve the neurological evaluation and study more precisely the EEGs from normal source (somatosensory cortex (SC) in parietal lobe) and AD sources (right amygdala (RA) and left amygdala (LA) in medial temporal lobe), (2) to give a preliminary quantitative estimation of errors due to varying sources and (3) the variations of EEG due to different brain tissue distortion levels to address the effects of different levels

Md R. Bashar is with the Department of Mathematics and Computing, University of Southern Queensland, QLD 4350, Australia (corresponding author to provide phone: 61-7-4631 1158; fax: 61-7-6431-5550; e-mail: bashar@ usq.edu.au).

Yan Li is with the Department of Mathematics and Computing, University of Southern Queensland, QLD 4350, Australia (e-mail: liyan@usq.edu.au).

Peng Wen is with the faculty of Engineering and Surveying, University of Southern Queensland, QLD 4350, Australia (e-mail: pengwen@usq.edu.au).

of dementia.

The paper is organized as follows. The Introduction Section describes background knowledge of AD along with its source positions. Head model construction, finite element conductivity, and source modeling are illustrated in Methods Section. Simulation and Experiment setup Section shows how to develop experimental environment. It also shows the way of analyzing EEGs by means of two statistical measurements. The analysis and visualization of obtained results (scalp potentials) are shown in Result Section. Finally, Discussion and Conclusion Section summarize and conclude our findings.

II. METHODS

A. Head Model Construction

Magnetic resonance imaging (MRI) is essential for constructing a realistic head model. We use T1 weighted MRI image of $149 \times 188 \times 148$ (x, y, z) dimensions and $1.00 \times 1.00 \times 100$ (x, y, z) resolutions having 8MB in disk size from BrainSuite2 [9]. We perform brain tissue segmentation from raw MRI using the following steps. Firstly, non-brain tissues are removed from the MRI using skull stripping. Secondly, the compensation for image non-uniformity is performed. Finally, each voxel is classified according to its tissue type [9]. Skull striping is addressed to identify brain and non brain voxels in MRI. It is done for the precaution to avoid voxel identifying critic. Because the measured signal intensities of brain tissues, such as white matter (WM), gray matter (GM) and cerebrospinal fluid (CSF) can overlap with those of other head tissues, such as skin, bone, muscle and fat. Skull striping is performed using a three-step procedure: (a) MRI processing to smooth non essential gradients using an anisotropic diffusion filter, (b) identifying anatomical boundaries using Marr-Hildreth edge detector and (c) objects identifying by a sequence of mathematical morphological operations. After skull striping, we then compensate for non-uniformity due to inhomogeneities in the magnetic fields, magnetic susceptibility variations in the scanned subject and other factors. Signal intensities measured at each voxel in an ideal MRI acquisition system will vary throughout the volume depending only on the tissues presenting at that location. However, MRI shows non-uniform tissue intensities in practice. Therefore, tissue labels cannot be reliably assigned to voxels and it requires non-uniformity compensation, which is performed by spatially slowly varying multiplicative bias field. The variations of bias fields are estimated by fitting a parametric tissue measurement model to the histograms of small neighborhoods. We then perform smoothing and interpolating using a regularized tricubic B –spline curve. Later on, each voxel intensity-normalized MRI is labeled using maximum a posterior classifier. This classifier combines the partial volume tissue measurement model with a Gibbs prior that models the spatial properties of brain tissue. The details of tissue classification are found in other studies [11-12]. Segmenting the brain tissues, we model scalp and skull using various threshold operators [12]. The details of realistic head construction are illustrated in our previous study [13]. These segmented head tissues are tessellated to be ready to assign conductivities and other forward computing steps. After assigning conductivities and positioning sources in the brain (discussed below), we perform forward computation using finite element method (FEM) [14-17] to construct a realistic head model. We measure the scalp potentials (EEG) based on the head model using 64 electrodes residing different places on the head surface.

B. Finite Element Conductivity

The tetrahedra or elements of head tissues are labelled according to their compartment memberships. The following isotropic conductivities [16-18] are assigned to the brain (σ_{brain}) = 0.33S/m, CSF (σ_{CSF}) = 1.0 S/m , skull (σ_{skull}) = 0.0042 S/ and scalp (σ_{scalp}) = 0.33 S/m. As AD caused reasoning the deposition of unsaturated tau protein in brain tissues, we adopt different head models assigning conductivity variations. We assume that tau protein consumes fat resistivity (reciprocal of conductivity). Haueisen et al. [19] measured resistivity of human head cell and found 2500 Ωcm mean value with 1500 Ωcm lower bound and 5000 Ωcm upper bound values for fat tissues. Awada et al. [20] accounted 0.02 S/m and 0.07 S/m conductivity values for fat tissues. Therefore, we assign 0.04 S/m conductivity mean values for the distorted brain tissue throughout this study.

C. Source Modelling

The dipole located at somatosensory cortex (SC) in parietal lobe is addressed as normal source and AD sources are addressed by the dipole positioned in right amygdala (RA) and left amygdala (LA) in hippocampus of medial temporal lobe. Figure 1 shows an example of a dipole location for RA source in MRI. We choose the dipole situated in SC as a reference dipole. Because it is known that parietal lobe integrates sensory information from different parts of a body. By surveying different literature [1-8], it is obvious that the source of AD resides in hippocampus. Therefore, we choose to set other sources either in RA or LA to understand how it would affect on EEG. We consider the dipole located in axial, coronal and sagittal planes with magnitude of 1 µA using equivalent current dipole (ECD) method.
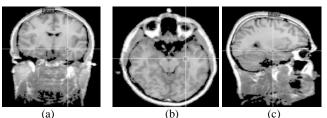

(a)   (b)   (c)

Fig. 1 Location of one of the AD sources in RA by the cross hairs in different views: (a) coronal, (b) axial and (c) sagittal.

III. SIMULATION AND SETUP

The realistic head model is implemented by taking MRI

slices as input, segmenting into several head tissue compartments, making mesh generation, assigning conductivity to the individual elements, putting source location inside the brain and performing forward computation. We perform MRI image segmentation using BrainSuite2. Segmenting the MRI, we generate mesh into 101K elements from 18K using online Tetgen® package [21]. Mesh generation provides 77966, 5123, 4711 and 13732 elements for the scalp, skull, CSF and brain tissue layers, respectively. We assign homogeneous isotropic conductivity to each tissue. We consider SC, RA and LA sources and 64 electrodes for the measurement of scalp potentials using FEM tool from BrainStorm2 online package [22,23]. We also developed other four realistic head models with 5%, 10%, 15% and 20% brain distortions.

The potentials on scalp are computed by means of 64 electrodes positioned at different places on a head surface using left ear-nasion-right ear alignment for both head models. The head model constructed from the SC source is addressed as reference model and other head models are addressed as computed models. These models are analyzed by calculating relative difference measure (RDM) [24] for the topology error (minimum error: RDM=0). As the RDM error compares the varying potential electrode by electrode, it doesn't provide the actual outline. Therefore, other types of errors, such as magnification (MAG) is indispensable analyzing the overall amplitude and magnitude difference values (minimum error: MAG=1) [24]. MAG error expresses either higher or less value than its reference. RDM and MAG are defined as [24]:

$$RDM = \sqrt{\sum_{i=1}^{N}\left(\frac{ref_i}{\sqrt{\sum_{i=1}^{N}ref_i}} - \frac{comp_i}{\sqrt{\sum_{i=1}^{N}comp_i}}\right)^2} \quad (1)$$

$$MAG = \sqrt{\frac{\sum_{i=1}^{N}comp_i^2}{\sum_{i=1}^{N}ref_i^2}} \quad (2)$$

where N represents the number of electrodes, ref represents electrode potentials for reference model and comp represents electrode potentials for the computed model.

The visualization of the obtained EEGs to observe the differences of scalp potentials produced by both models is also shown in this study. It is performed by adopting and feeding our obtained EEGs to advanced source analysis (ASA) system [25]. ASA is a software package designed for functional brain imaging based on EEG/MEG measurements.

IV. RESULTS

We first compare the scalp potentials obtained from two AD sources (RA and LA) to those of normal (SC) sourced EEG. We find that RA and LA sourced potentials result in 61.97% to 197.12% RDM errors, and 0.21 to 0.07 MAG

errors, respectively. Analyzing these errors, we find that the scalp potentials originated from AD sources differ from SC source and also exhibit less scalp potentials.

Figure 2 shows RDM and magnification (MAG) errors where scalp potentials of computed head models are from different brain tissue distortion levels (BTDLs). For instance, we have used the EEGs obtained from 5% BTDL for SC, RA and LA sources as computed model to the EEGs obtained from without BTDL for corresponding sources, respectively. Similarly, we perform same computations for other BTDLs. RDM errors are between 10% and 28% and MAG errors are in the range of 0.98 to 1.09. RA sourced BTDLs show higher RDM and SC sourced BTDLs show higher MAG errors. We find that 10% distortion level is more sensitive than other BTDLs in respect to both RDM and MAG.
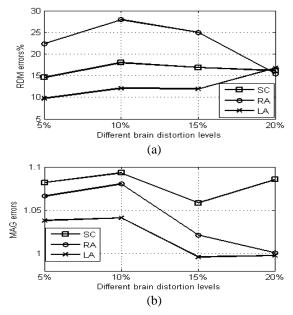

(a)

(b)

Fig. 2 RDM (a) and MAG (b) errors from different brain tissue distortion levels on source to source basis.

Figure 3 shows RDM and MAG errors where AD sourced scalp potentials are compared to SC sourced EEG. In Figure 3, normal represents a model without any brain tissue distortion. RA shows 59% to 61% RDM and 0.21 to 0.23 MAG errors, while 197% RDM and 0.076 to 0.08 MAG errors are shown by LA sourced EEG. We observe that RA generates less RDM and MAG errors than LA.

Figure 4 shows the contour map of scalp potentials resulted from different realistic head models. Analyzing the contour maps, we found that the scalp potentials generated by various brain distortion levels are different from the reference model and are significantly varying from each other.
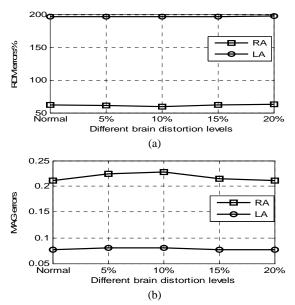
(a)

(b)

Fig. 3 RDM (a) and MAG (b) errors from RA and LA sourced without and with different brain tissue distortion levels to SC sourced normal EEG.
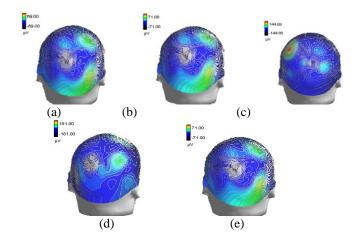

(a) (b) (c)

(d) (e)

Fig. 4 Contour view of scalp potentials obtained from somatosensory cortex (a) reference model, (b) five percent, (c) ten percent, (d) fifteen percent and (e) twenty percent brain tissue distortions.

V. DISCUSSION

In this study, we observe the significant changes on scalp potentials by means of RDM and MAG using the forward computation for the sources in AD region with those of normal source region by constructing realistic head models to assist the clinicians. We also implement 5%, 10%, 15% and 20% brain tissue distortions to address different stages of dementia, such as predementia, early dementia, moderate dementia and advanced dementia, respectively.

Comparing the EEGs obtained from AD sources to SC sourced EEG; we found the differences of scalp potentials due to the changing of the sources. Similarly, different levels of brain tissue distortion also cause substantial potential changes. In most of the cases, MAG errors generated by SC source for different brain distortion levels show higher values than those

of AD sourced EEG (Figure 2(b)). The reason is the position of sources. When a source is closer to the cortex, the distance between the source and the sensor is minimum. Therefore, more potential is found on sensor than the source at the deeper brain region. We also implement two different AD sources in right amygdala and left amygdala to show the changing of EEGs in order to source position.
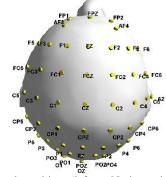

Fig. 5 Electrode positions (left ear-Nasion – right ear). Odd number with electrode names indicate left hemisphere, even number with electrode names indicate right hemisphere.

Visualization of scalp potentials (shown in Figure 4) is carried out based on our obtained results associating with ASA for 10-20 electrode system. A head model with electrodes is shown in Figure 5. Though all electrodes are not visible, electrodes are addressed by different names with 'F' for frontal lobe, 'P' for parietal lobe, 'O' for occipital lobe and 'T' for temporal lobe. Combining the concepts of electrode positions and scalp potentials, it is apparent that the electrodes in the source region are more sensitive to the electrodes in other regions. When the source is placed in somatosensory cortex, it spreads the potentials to its nearest electrodes positioning in central parietal region. Therefore, the electrodes are in parietal and temporal show more potential when dipole is in hippocampus.

VI. CONCLUSION

In this study, we find that scalp potentials generated from AD sources differ and produce less value than normal source. Different brain distortion levels also cause substantial potential changes. It is also found that the electrodes positioned in the source regions are more sensitive than other electrodes. We conclude that this study would assist analyzing scalp potentials for diagnosis as well as awareness of different stages of AD patients.

REFERENCES

[1] S. Kloppel, C. M. Stonnington, C. Chu , B. Draganski, R. I. Scahill, J. D. Rohrer, N. C. Fox, C. R. Jack Jr, J. Ashburner and R. S. J. Frackowiak, "Automatic classification of MR scans in Alzheimer's disease," *Brain*, vol. 131, pp. 681-689, Jan. 2008.

[2] L. Mosconi, S. Sorbi, M. J. de Leon, Y. Li , B. Nacmias, and P. S. Myong, "Hypometabolism exceeds atrophy in presymptomic early-onset familial Alzheimer's disease," *Journal of Neuclear Medicine*, vol. 47, pp. 1778-1786, Nov. 2006.

[3] J. C. Baron, G. Chetelat, B. Desgranges, G. Perchey, B. Landeau, V. de la Sayette, and F. Eustache, "In vivo mapping of gray matter loss with voxel-based morphometry in mild Alzheimer's disease," *NeuroImage*, vol. 14, pp. 298–309, Aug. 2001.

[4] A. D. Smith, and K. A. Jobst, "Use of structural imaging to study the progression of Alzheimer's diseases," *British Medical Bulletin*, vol. 52, no. 3, pp. 575-586, 1996.

[5] M. Chupi, A. R. Mukuna-Bantumbakulu, D. Hasboun, E. Bardinet, S. Baillet, S. Kinkingnehun, L. Lemieux, B. Dubois, and L. Garnero, , "Anatomically constrained region deformation for the automated segmentation of the hippocampus and amygdala: Method and validation on controls and patients with Alzheimer disease," *NeuroImage*, vol. 34, pp. 996-1019, Feb. 2007.

[6] T. Patel, R. Polikar, C. Davatzikos, and C. M. Clark, "EEG and MRI Data Fusion for Early Diagnosis of Alzheimer's Diseas," in *proc. 30th Annual International IEEE EMBS Conference,* Canada, 2008, pp. 1757-1760.

[7] R. Polikar, T. D. Green, J. Kounios, and C. M. Clark, "Comparative multiresolution wavelet analysis of ERP spectral bands using an ensamble of classifier approach for early diagnosis for Alzheimer's disease," *Computers in. Biology and Medicine*, vol. 37, no. 4, pp. 542-558, Apr. 2007.

[8] G. Chetelat, B. Desgranges, B. Landeau, F. Mezenge, J. B. Poline, V. de la Sayette, F. Viader, F. Eustache, and J. C. Baron, "Direct voxel-based comparison between grey matter hypometabolism and atrophy in Alzheimer's disease," *Brain,* vol. 131, pp. 60-71, Jan. 2008.

[9] (Online source) D. W. Shattuck. (2005). *BrainSuite 2 Tutorial*. Available: http://brainsuite.usc.edu

[10] D. W. Shattuck, S. R. Sandor-Leahy, K. A. Schaper, D. A. Rottenberg, and R. M. Leahy,"Magnetic Resonance Image Tissue Classification Using a Partial Volume Model," *NeuroImage*, vol. 13, no. 5, pp. 856-876, 2001.

[11] D. W. Shattuck, and R. M. Leahy, "BrainSuite: An Automated Cortical Surface Identification Tool," *Medical Image Analysis*, vol. 8, no. 2, pp. 129-142, June 2002.

[12] B. Dogdas, D. W. Shattuck, and R. M. Leahy, "Segmentation of Skull and Scalp in 3-D Human MRI using Mathematical Morphology," *Human Brain Mapping*, vol. 26, pp. 273-285, June 2005.

[13] M. R. Bashar, Y. Li, and P. Wen, "EEG analysis on skull conductivity perturbations using realistic head model," *Lecture Notes on Computer Science*, vol. 5589, pp. 208-215, July 2009.

[14] R. N. Klepfer, C. R. Johnson, and S. M. Robert, "The effects of Inhomogeneities and Anisotropies on Electrocardiographic Fields: A 3-D Finite –element Study," *IEEE Transactions on Biomedical Engineering*, vol. 44, no. 8, pp. 706-719, Aug. 1997.

[15] C. H. Wolters, "Influence of Tissue Conductivity Inhomogeneity and Anisotropy on EEG/MEG based Source Localization in the Human Brain," PhD thesis. University of Leipzig. France; July 2003.

[16] M. R. Bashar, Y. Li, and P. Wen, "Influence of white matter inhomogeneous anisotropy on EEG forward computing," *Australasian Physical & Engineering Sciences in Medicine*, vol. 31, no. 2, pp. 122-130, 2008.

[17] P. Wen P, and Y. Li, "EEG human head modelling based on heterogeneous tissue conductivity," *Australasian Physical & Engineering Sciences in Medicine*, vol. 29, no. 3, pp. 235-240, 2006.

[18] D. Gullmar, J. Haueisen, M. Wiselt, F. Giebler, L. Flemming, A. Anwander, T. R. Knosche, C. H. Wolters, M. Dumpelmann, D. S. Tuch and J. R. Reichenbach., "Influence of Anisotropic Conductivity on EEG source Reconstruction: Investigations in a Rabbit Model," *IEEE Transactions on Biomedical Engineering*, vol. 53, no. 9, pp. 1841-1850, Sep. 2006.

[19] J. Hauseisen, C. Ramon, M. Eiselt, H. Brauer, and H. Nowak,"Influence of Tissue Resistivities on Neuromagnetic Fields and Electric Potentials studied with a Finite Element Model of the Head," *IEEE Transactions on Biomedical Engineering*, vol. 44, no. 8, pp. 727-735, Aug. 1997.

[20] K. A. Awada, S. B. Baumann, and D. R. Jackson," Effect of conductivity uncertainties on EEG source localization using a 2D finite element model," in *Proc. of 19th International Conference – IEEE/EMBS*, USA, 1997, pp. 2124-2127.

[21] (Online Source) H. Si. (2004). *TetGen*. Available: http://tetgen.berlios.de

[22] S. Baillet, J. C. Mosher, and R. M. Leahy, "Electromagnetic Brain Imaging using Brainstorm," in *Proc. IEEE Int. Symposium on Biomed. Eng.: Macro to Nano* 2004, pp. 652-655.

[23] G. B. Frisoni, C. Pievani, C. Testa, S. F. Francesca, L. Bresciani , M. Bonetti, A. Beltramello, K. M. Hayashi, A. W. Toga, and P. M. Thompson, "The topography of grey matter involvement in early and late onset Alzheimer's disease," *Brain*, vol. 130, pp. 720-730, Feb. 2007.

[24] J. W. Meijis, O. W. Weier, M. J. Peters, and A. van Oosterom, "On the numerical accuracy of the boundary element method," *IEEE Transactions on Biomedical Engineering*, vol. 36, no. 10, pp. 1038-1049, Oct. 1989.

[25] (Online Source) ANT Software, The Netherland. (2007). *Advanced Source Analysis*. Available: www.ant-neuro.com